Time Dependent Simulation of PD Electromagnetic Wave Propagation in GIS Systems

Tao Zhao[1, 2], Martin D. Judd[3] and Brian G. Stewart[2]
[1]North China Electric Power University [2]University of Strathclyde [3]High Frequency Diagnostics Ltd
204 George Street
Glasgow, G1 1XW UK

***Abstract*- UHF methods have been widely used in PD detection and localization in GIS systems. Modeling of electromagnetic wave propagation inside a GIS structure can be helpful for understanding and improvement in sensitivity of PD detection by providing information to help determine more optimal positions for UHF PD sensors. This paper studies the effect of L-type and T-type GIS structures on electromagnetic wave propagation by simulating the time dependent wave propagation behavior for these arrangements of the GIS busbar. The effects of L-type and T-type structures for PD electromagnetic wave propagation behavior are presented. It is noted that if the location of the electric field detected by a UHF sensor is chosen reasonably based on knowledge of the physical structures, the measurement result obtained can reduce the attenuation affects introduced by the L-type and T-type structure.**

I. INTRODUCTION

The ultra-high frequency (UHF) technique has been widely used for many years to detect partial discharge (PD) in gas-insulated systems (GIS), by which both PD detection and location can be realized [1-3]. This technique is also much more practical for on-site use, being less sensitive to noise and more effective for PD location compared with the conventional method according to IEC 60270. Nonetheless, many factors act to prevent reaching high accuracy for PD detection and location. First, a calibration to "apparent charge in pC" is not possible due to the complex PD pulse propagation characteristics, and second the PD detection sensitivity depends on various parameters like the distance between the PD defect and the sensor.

To overcome the issues above, a technical brochure [4] published by CIGRE in 2016 collected available experience on PD sensitivity verification and described its practical applications for GIS. A detailed description of the two-step procedure is given and as a guideline, it assists manufacturers and users in the effective application of the UHF method for PD detection on GIS.

From a general point of view, GIS can be considered as having a coaxial waveguide geometry with its central internal HV conductor and grounded enclosure. In a practical installation, there are not only linear structures, but also many L-type and T-type structures. Propagation characteristics of a PD electromagnetic (EM) wave in GIS are complicated. When the EM wave spreads in the GIS system, several phenomena may occur (such as reflection, refraction, resonance, wave mode conversion and attenuation), which combine to cause complex EM wave behavior [4-6].

Many research investigations have been conducted to explore the behavior of EM waves generated by PD inside GIS. Okabe et al. [7, 8] investigated the reflection and mode conversion of EM waves in various GIS structures. Based on simulations in their High Frequency Structure Simulator, the propagation characteristics of multiple modes of an EM wave in GIS structures were illustrated. Hikita et al. [9-11] analyzed the EM attenuation trend through a spacer, an L-shaped branch, and a T-shaped branch by means of both simulation and experiments. They concluded that the attenuation trend was mainly due to superimposition of the TE mode and the TEM mode. Behrmann et al. [12-13] explored EM wave behavior inside GIS by performing RF network analyzer measurements and 3D finite-element modeling. Their results show that refinements to finite element modelling (FEM) techniques result in a closer match to actual measurements.

It is valuable to understand EM wave behavior in GIS systems for the purpose of improving the utilization and allocation of UHF sensors in PD detection. Therefore, this paper is devoted to building 3D finite element models for L-type and T-type structures for time dependent simulation investigations to understand the propagation behavior of EM waves in GIS systems. Specifically, two effects are explored: the reflection effect of EM wave propagation and the effect of L-type and T-type structures on the most effective positioning of UHF sensors for detecting PD signals that have propagated through them.

II. SIMULATION MODEL

The geometry of the L-type GIS structure used in this study is shown schematically in Fig. 1. The inner and outer diameters of the conductor and tank are 125 mm and 420 mm respectively [7]. The conductors are represented as perfect electric conductors (PEC) in the model created in COMSOL Multiphysics software. Sulfur hexafluoride (SF_6) is the insulation gas considered (relative permittivity ε_r = 1, relative permeability μ_r = 1, electrical conductivity σ = 0). Dielectric spacers are considered as epoxy resin (relative permittivity ε_r = 4, relative permeability μ_r = 1, electrical conductivity σ = 0). The field formulation used for the time-domain simulations is described by the following equations [13-14]:

$$\nabla \times \left(\frac{1}{\mu_r} \nabla \times \mathbf{A} \right) + \mu_0 \sigma \frac{\partial \mathbf{A}}{\partial t} + \mu_0 \frac{\partial}{\partial t} \left(\varepsilon_0 \varepsilon_r \frac{\partial \mathbf{A}}{\partial t} \right) = 0 \quad (1)$$

$$\mathbf{n} \times \mathbf{E} = 0 \text{ (PEC boundary condition)} \quad (2)$$

$$Z_{port} = \frac{U_{port}}{I_{port}} \quad \text{(Lumped port with voltage input)} \qquad (3)$$

$$\mathbf{A}(\mathbf{r}, 0) = 0 \quad \text{(Zero initial condition)} \qquad (4)$$

where **A** is the magnetic vector potential, μ_0 represents the magnetic permeability of vacuum, μ_r is the relative magnetic permeability, ε_0 is the electric permittivity of vacuum, ε_r refers to the relative permittivity of the propagation medium, **n** is a unit vector normal to the surface and Z_{port} is the wave impedance of the lumped (input) port. The output port is set to a scatter boundary for modeling an open boundary and this boundary is transparent for incoming plane waves with any angle of incidence. Therefore there is no reflection back into the structure at the output port during the simulation.

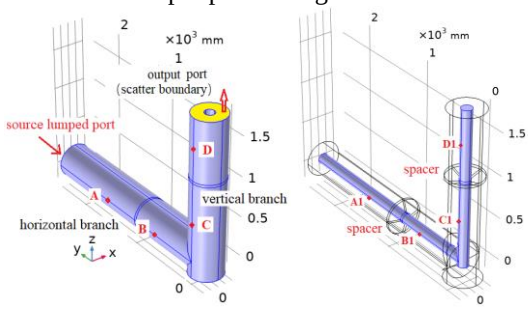

(a) (b)

Fig. 1. L-type structure with two spacers and the locations of the point probes. (a) Geometry of outer conductor. (b) Geometry of inner conductor.

TABLE 1 Coordinates of the point probes in Fig.1.

A	(-210, 1500, 0)	A1	(-62.5, 1500, 0)
B	(-210, 500, 0)	B1	(-62.5, 500, 0)
C	(-210, 0, 500)	C1	(-62.5, 0, 500)
D	(-210, 0, 1500)	D1	(-62.5, 0, 1500)

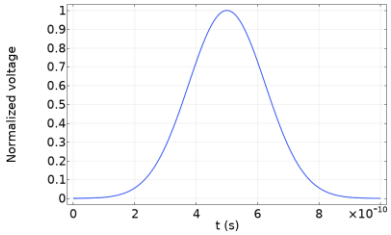

Fig. 2. The Gaussian pulse at the source port

To model a PD source, a Gaussian pulse with half amplitude width of 0.3 ns is used at the source lumped port as shown in Fig. 2 [5-6]. The time domain expression of the pulse is represented by the following equation:

$$V(t) = V_0 e^{-\frac{t^2}{2\tau^2}} \qquad (5)$$

where V_0 is the amplitude of the pulse, and τ is a parameter determining the pulse width. Because of the stochastic nature of PD, the amplitude of PD pulse is variable. Therefore, for the purpose of simulation, the model uses a normalized PD pulse amplitude and the electric field results are presented on a similarly normalized amplitude scale.

Point probes that record the evolution of electric field values during the simulation were set with positions shown as red points in Fig. 1. Coordinates of these point probes are listed in Table 1. Time dependent plots of the electric field in the radial direction during a time range [0, 0.1, … 20 ns] are produced once the simulation is complete.

The geometry of the T-type GIS structure is presented in Fig. 3, which also shows the point probe positions. Coordinates of these point probes are the same as in Fig. 1 and Table 1.

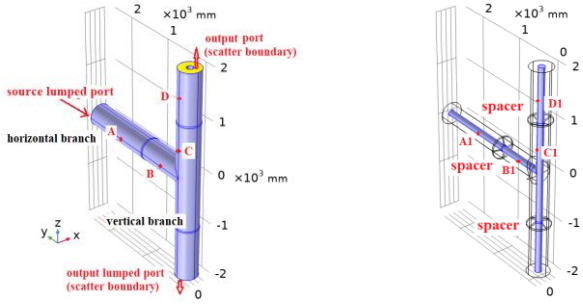

(a) (b)

Fig. 3. T-type structure with three spacers and the locations of the point probes. (a) Geometry of outer conductor. (b) Geometry of inner conductor.

III. Simulation Results

A. *L-type structure*

Fig. 4 shows the time-varying electric field at the point probes on the horizontal and vertical branches of the L-type structure, while Fig. 5 shows a snapshot the electric field distribution in the structure at t = 7.8 ns. The propagation and reflection of EM waves are also illustrated in Fig. 4 and Fig. 5. The curves in Fig. 4 show the electric field at the point probes is zero at the beginning of simulation time. When the EM wave passes each point probe, there is a peak in the curve. After that, the curves start to fluctuate over time and there are many peaks with lower amplitudes generated by the reflection effect of the spacers and L bend.

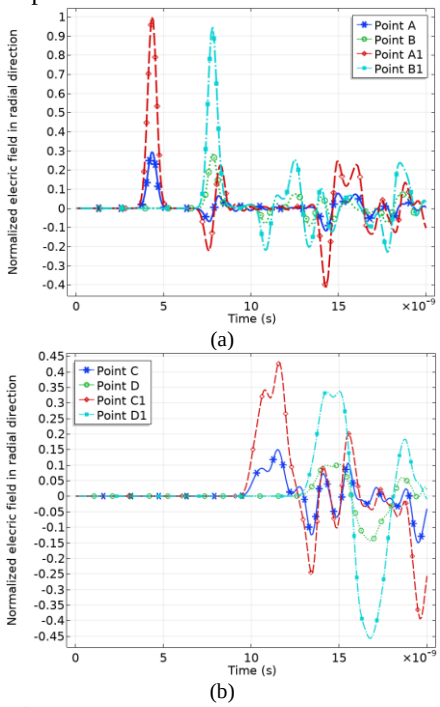

(a)

(b)

Fig. 4. Electric field in radial direction versus time (the maximum on point A1 is as the normalized benchmark). (a) Point probes on horizontal branch. (b) Point probes on vertical branch.

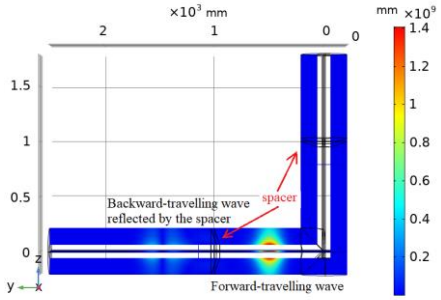

Fig. 5. Electric field distribution at the time of t = 7.8 ns

From the reflected waves in the plot, it can be seen that the spacer reflects a small amount of wave energy as displayed in Fig. 5. In this model, after passing through one spacer, the amplitude of the electric field decreases by about 5%. As the reflected wave propagates, the waveform begins to become more undulating.

Fig. 4(b) describes the electric field variation during the process of the EM wave passing by the corner of the L-type structure. It shows different characteristics when the EM wave propagates into the vertical branch. The change of waveform and amplitude indicates overlap of adjacent waves caused by the wave reflection. The electric field in Fig. 4(b) reveals that the electric field properties differ quite significantly for different positions. Therefore, for electric field detection, the outputs of UHF PD sensors may be very different for different sensor installation locations.

Fig. 6 and Table 2 compare the difference of the electric field for different positions. The coordinates of these positions are given in Fig. 7 (it should be noted that these locations are commonly used for PD sensor installations [8, 15]).

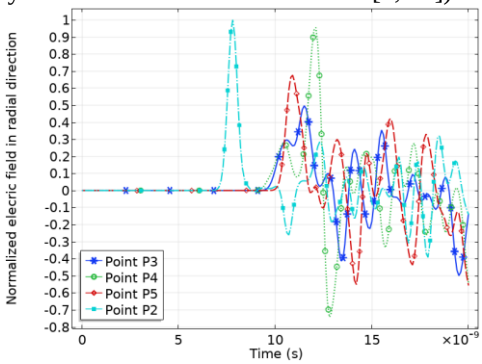

Fig. 6. Electric field in radial direction versus time at test position points (the maximum on point P2 is as the normalized benchmark).

TABLE 2 Attenuation of EM wave passing by the corner of L type

Point probe positions	Normalized electric field in radial direction
P1 (-210, 500, 0)	98%
P2 (0, 500, 210)	100%
P3 (-210, 0, 500)	51%
P4 (0, 210, 500)	98%
P5 (0, -210, 500)	69%

In Table 2, the maximum difference of the peak values at the test point locations P3, P4 and P5 is up to 47%. Therefore, for electric field detection, it is notable that if the EM wave signal passes through the L-type structure and is detected by the sensor, the installation position of the sensor will affect the strength of the received signal. It is indicated by comparison that the attenuation at test point P3 is the most significant and the detection sensitivity is higher at the other two test points P4 and P5 in horizontal direction if the drawing direction of the tank is defined to be the horizontal direction. Therefore, if the location of the sensor is chosen reasonably, the measurement sensitivity will almost be unaffected by the L-type structure.

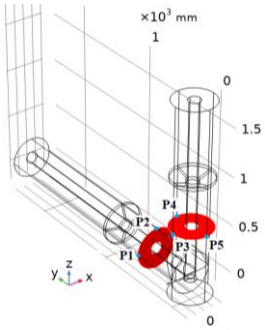

Fig.7. Test point positions commonly used for sensor installations

B. *T-type structure*

Fig. 8 shows the time-varying electric field at the point probes on the horizontal and vertical branches of the T-type structure. Similar to the results of L-type structure, it also shows different characteristics when the EM wave propagates into the vertical branch of T-type structure. The change of waveform and amplitude indicates overlap of adjacent waves caused by the wave reflection. The electric field in Fig. 8(b) reveals that the electric field properties differ quite significantly for different positions.

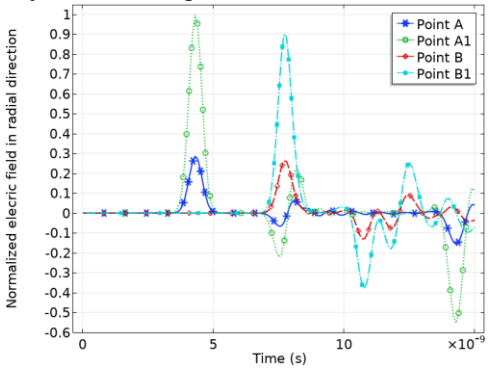

(a)

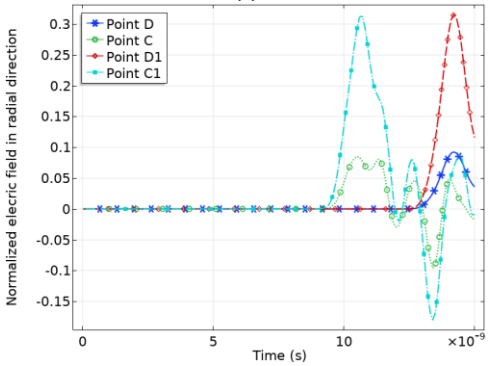

(b)

Fig. 8. Electric field in radial direction versus time at point probes (the maximum on point A1 is as the normalized benchmark). (a) Point probes on horizontal branch. (b) Point probes on vertical branch.

The difference of the electric field for different positions are compared in Fig. 9 and Table 3. The coordinates of these positions are shown in Fig. 10. In Table 3, the maximum difference of the peak values at tested locations of P3, P4 and P5 is up to 50%. Therefore, for the electric field detection, it is noted that if the EM wave signal passes through the T-type structure and is detected by the sensor, the installation position of the sensor will affect the strength of the received signal. By comparison, a result similar to the L-type situation is also obtained. The most significant attenuation takes place at test point P3 and the detection sensitivity is higher at the other two test points P4 and P5 in horizontal direction of the L bend if the drawing direction of the tank is defined to be the horizontal direction. Therefore, if the location of the sensor is chosen reasonably, the measurement sensitivity obtained can reduce the attenuation affected by the T-type structure.

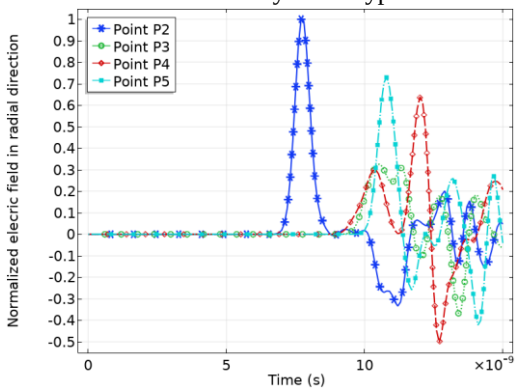

Fig. 9. Electric field in radial direction versus time at test point positions

TABLE 3 Attenuation of EM wave passing by the corner of T type

Point probe positions	Normalized electric field in radial direction
P1 (-210, 500, 0)	100%
P2 (0, 500, 210)	100%
P3 (-210, 0, 500)	37%
P4 (0, 210, 500)	63%
P5 (0, -210, 500)	73%

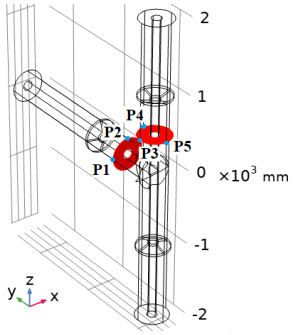

Fig. 10. Tested positions commonly used for sensor installations

IV. Conclusions

In this study, the effects of L-type and T-type GIS structures on the propagation behavior of EM waves excited by PD have been investigated. Changes of waveform and amplitude were observed in both L- and T-type structures during the process of EM wave propagation. The simulations indicate an overlap of adjacent waves caused by wave reflection so that the time-varying electric field differs quite significantly for different positions at which UHF PD sensors might be mounted. Therefore, appropriate selection of sensor installation positions relative to the L- and T-type arrangements of GIS bus bars might ensure a more consistent PD detection sensitivity.

It is indicated by comparison that the detection sensitivity at the test point in the horizontal direction (0 °) of the L bend and T bend is higher than that in the vertical direction (90 °) if the drawing direction of the tank is defined to be the horizontal direction (0 °). Therefore, if the location of the electric field detected by the sensor is chosen reasonably, the measurement sensitivity obtained can minimize the effects of attenuation introduced by the L-type and T-type structure.

References

[1] J. S. Pearson, O. Farish, B. F. Hampton, M. D. Judd, D. Templeton, B. M. Pryor and I. M. Welch, "Partial discharge diagnostics for gas insulated substations," *IEEE Trans. Dielectr. Electr. Insul.*, vol. 2, no. 5, pp. 893-905, Oct. 1995.

[2] G. Behrmann, W. Koltunowicz and U. Schichler, "State of the Art in GIS PD Diagnostics," *2018 Condition Monitoring and Diagnosis (CMD)*, Perth, WA, 2018, pp. 1-6.

[3] CIGRE WG D1.33, Tech. Brochure 502, "High-Voltage On Site Testing with Partial Discharge Measurement," 2012.

[4] CIGRE WG D1.25, Tech. Brochure 654, "UHF partial discharge detection system for GIS: Application guide for sensitivity verification," 2016.

[5] M. D. Judd and O. Farish, "High bandwidth measurement of partial discharge current pulses," *Proc. IEEE Int. Symp. Elect. Insul.*, vol. 2, pp. 436–439, Jun. 1998.

[6] M. D. Judd, O. Farish and B. F. Hampton, "The excitation of UHF signals by partial discharges in GIS," *IEEE Trans. Dielectr. Electr. Insul.*, vol. 3, no. 2, pp. 213-228, April 1996.

[7] S. Kaneko, S. Okabe, M. Yoshimura, et al, "Partial discharge diagnosis method using electromagnetic wave mode transformation in actual GIS structure," IEEE Trans. Dielectr. Electr. Insul., vol. 15, no. 5, pp. 1329-1339, Oct. 2008.

[8] S. Okabe, S. Kaneko, M. Yoshimura, et al, "Partial discharge diagnosis method using electromagnetic wave mode transformation in gas insulated switchgear," *IEEE Trans. Dielectr. Electr. Insul.*, vol. 14, no. 3, pp. 702–709, Jun. 2007.

[9] M. Hikita, S. Ohtsuka, G. Ueta, et al, "Influence of insulating spacer type on propagation properties of PD-induced electromagnetic wave in GIS," *IEEE Trans. Dielectr. Electr. Insul.*, vol. 17, no. 5, pp. 1642–1648, Oct. 2010.

[10] M. Hikita, S. Ohtsuka, J. Wada, et al, "Propagation properties of PD-induced electromagnetic wave in 66 kV GIS model tank with L branch structure," *IEEE Trans. Dielectr. Electr. Insul.*, vol. 18, no. 5, pp. 1678–1685, Oct. 2011.

[11] M. Hikita, S. Ohtsuka, T. Hoshino, et al, "Propagation properties of PD-induced electromagnetic wave in GIS model tank with T branch structure," *IEEE Trans. Dielectr. Electr. Insul.*, vol. 18, no. 1, pp. 256–263, Feb. 2011.

[12] G. Behrmann, S. Franz, J. Smajic, et al, "UHF PD signal transmission in GIS: Effects of 90 ° bends and an L-shaped CIGRE step 1 test section," *IEEE Trans. Dielectr. Electr. Insul.*, vol. 26, no. 4, pp. 1293–1300, 2019.

[13] G. Behrmann, K. Wyss, J. Weiss, et al, "Signal delay effects of solid dielectrics on time-of-flight measurements in GIS," *IEEE Trans. Dielectr. Electr. Insul.*, vol. 23, no. 3, pp. 1275–1284, 2016.

[14] J. Smajic, W. Holaus, J. Kostovic, et al, "3D Full-Maxwell Simulations of Very Fast Transients in GIS," *IEEE Trans. on Magnetics*, vol. 47, no. 5, pp. 1514-1517, May 2011.

[15] G. Behrmann and J. Smajic, "RF PD signal propagation in GIS: Comparing S-parameter measurements with an RF transmission model for a short section of GIS," *IEEE Trans. Dielectr. Electr. Insul.*, vol. 23, no. 3, pp. 1331–1337, 2016.